Preprint Title	Development of fluorinated benzils and bisbenzils as room-temperature phosphorescent molecules
Authors	Shigeyuki Yamada, Takuya Higashida, Yizhou Wang, Masato Morita, Takuya Hosokai, Kaveendra Maduwantha, Kaveenga R. Koswattage and Tsutomu Konno
Publication Date	23 Mär 2020
Article Type	Full Research Paper
Supporting Information File 1	SI-S.YAMADA.pdf; 4.6 MB
ORCID® iDs	Shigeyuki Yamada - https://orcid.org/0000-0002-6379-0447; Takuya Hosokai - https://orcid.org/0000-0001-9164-4159

Development of fluorinated benzils and bisbenzils as room-temperature phosphorescent molecules

Shigeyuki Yamada*[1], Takuya Higashida[1], Yizhou Wang[1], Masato Morita[1], Takuya Hosokai[2], Kaveendra Maduwantha[2,3], Kaveenga Rasika Koswattage[2,3] and Tsutomu Konno[1]

Address: [1]Faculty of Molecular Chemistry and Engineering, Kyoto Institute of Technology, Matsugasaki, Sakyo-ku, Kyoto 606-8585, Japan; [2]National Metrology Institute of Japan, National Institute of Advanced Industrial Science and Technology, 1-1-1 Umezono, Tsukuba 305-8560, Japan and [3]Faculty of Technology, Sabaragamuwa University of Sri Lanka, P.O. Box 02, Belihuloya 70140, Sri Lanka

Email: Shigeyuki Yamada – syamada@kit.ac.jp

* Corresponding author

Abstract

Pure organic phosphorescent molecules are attractive alternatives to transition metal complexes-based phosphores for biomedical and technological applications owing to their abundance and nontoxicity. This article discloses the design, synthesis, and photophysical property of fluorinated benzil and bisbenzil derivatives as potential pure organic room-temperature phosphorescent molecules. These compounds were separately converted from the corresponding fluorinated bistolanes via $PdCl_2$-catalyzed oxidation by dimethyl sulfoxide, while non-fluorinated bistolane provided the corresponding bisbenzil derivatives exclusively in a similar manner. Intensive

investigation of the photophysical properties of the benzil and bisbenzil derivatives in toluene at 25 °C showed both fluorescence with a photoluminescence (PL) band at a maximum wavelength (λ_{PL}) of around 400 nm and phosphorescence with a PL band at a λ_{PL} of around 560 nm. Interestingly, intersystem crossing effectively caused fluorinated benzils to emit phosphorescence, which may be due to immediate spin-orbit coupling involving the $^1(n, \pi)\rightarrow{}^3(\pi, \pi)$ transition, unlike the case of fluorinated or non-fluorinated bisbenzil analogues. These findings would become useful tool to develop novel pure organic room-temperature phosphorescent materials.

Keywords

alkyne-oxidation; benzils; bistolanes; fluorinated compounds; phosphorescence

Introduction

The development of organic light-emitting molecules is recognized as one of the most important studies because of the broad application of these compounds as fluorescence probes, bio-imaging materials, and bio-sensors in the biomedical field [1–4] and as organic light-emitting diodes in the technological field [5–8]. Among the organic light-emitting molecules developed thus far, extended π-conjugated compounds (e.g., pyrenes and perylenes) emit fluorescence, which is a radiative deactivation process from the lowest singlet (S_1) excited state to the ground (S_0) state [9]. Interestingly, for such π-conjugated molecules, suitable structural modification can switch the radiative $S_1\rightarrow S_0$ process to another radiative deactivation process from the triplet (T_1) excited state to S_0 via an $S_1\rightarrow T_1$ intersystem crossing (ISC), resulting in the emission of phosphorescence [9].

Phosphorescent molecules generate two excitons (i.e., 25% S_1 excitons and 75% T_1 excitons) by application of an electric field, well-known for organic light-emitting diodes. S_1 excitons are converted to T_1 excitons via an ISC, finally achieving an excellent light-emitting efficiency (up to 100%) [10]. Therefore, extensive investigations to develop phosphorescent molecules have been performed thus far [11–13].

It has been established thus far that the construction of transition metal complexes containing a heavy atom that can promote an ISC process by a heavy metal effect (e.g., Ru [14], Ir [15,16], Pt [17], and Au [18–21]) (Figure 1A) is a possible molecular design for phosphorescence emission. However, it is strongly necessary to explore alternatives to rare metals because of the latter's scarcity and toxicity. Owing to recent considerable efforts, several molecular designs have been proposed as alternatives, particularly the use of pure organic phosphorescent molecules [22].

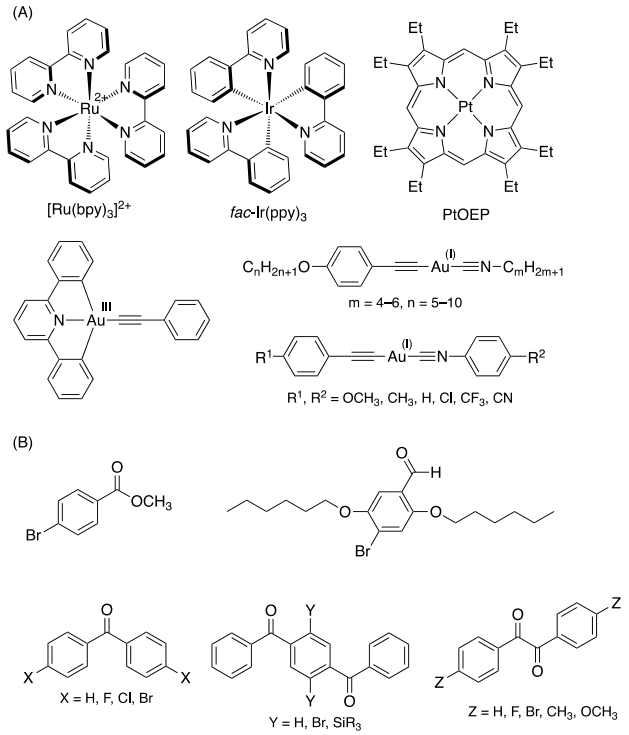

Figure 1: (A) Transition-metal-containing and (B) pure organic phosphorescent materials reported thus far (bpy: 2,2'-bipyridine, ppy: 2-phenylpyridine, OEP: octaethylporphyrin).

For example, methyl 4-bromobenzoate (Figure 1B) exhibits phosphorescence in crystalline form via nonradiative ISC to the T_1 state owing to crystallization-induced restriction of intramolecular motions [23]. Moreover, the crystalline 2,5-dihexyloxy-4-bromobenzaldehyde displays green phosphorescence, which stems from a quick ISC due to the heavy atom effect via halogen bonding (C=O···Br) [24]. Moreover, benzophenone- or benzil-type molecules can achieve long-lived phosphorescence owing to significant acceleration of spin-orbit coupling based on the El-Sayed rule involving the $^1(n, \pi) \rightarrow ^3(\pi, \pi)$ transition [25,26].

Over the past few years, our group has intensively investigated fluorinated 1,4-bis(2-phenylethyn-1-yl)benzenes (**1**), called bistolanes (Figure 2A), which show

prominent fluorescence not only in dilute solution, but also in the crystalline state [27–31].

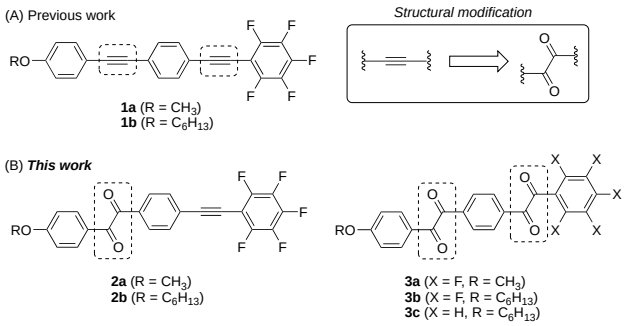

Figure 2: (A) Chemical structures of fluorescent bistolane derivatives previously developed by our group and (B) phosphorescent molecular structures intended for this work.

As a powerful tool to develop novel pure organic phosphorescent molecules, we envisioned the structural modification of the carbon-carbon triple (C≡C) bond in fluorinated bistolane **1** via oxidation to form the corresponding benzil (**2**) and/or bisbenzil (**3**) derivatives (Figure 2B). A literature review reveals that bisbenzil-type analogues have not received much attention, despite several publications on benzil-type phosphorescent molecules [25,26,32]. In this study, therefore, we examined the synthesis of novel benzil- and bisbenzil-type molecules via oxidation of fluorinated and non-fluorinated bistolane derivatives and evaluated their photophysical properties in detail.

Results and Discussion

Synthesis

Our study was initiated with the synthesis of fluorinated bisbenzil derivatives. According to the reported procedure [33,34], the $PdCl_2$-catalyzed oxidation of the C≡C bonds in **1** by dimethyl sulfoxide (DMSO) was performed (Scheme 1).

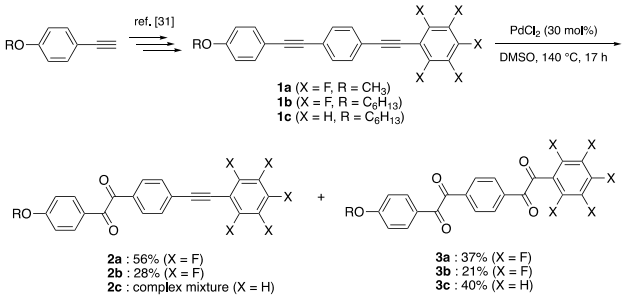

Scheme 1: Synthetic pathway for fluorinated benzil (**2**) and bisbenzil (**3**) derivatives.

The methoxy-substituted fluorinated bistolane **1a** was prepared from commercially available 4-ethynylanisole in four facile steps. Interestingly, stirring **1a** in DMSO solution in the presence of 30 mol% of $PdCl_2$ at 140 °C for 17 h produces two products (56% yield for the less polar product and 37% yield for the more polar one) after purification with column chromatography. Spectroscopic analyses (i.e., ^{1}H, ^{19}F, and ^{13}C nuclear magnetic resonance (NMR) spectroscopy, infrared spectroscopy, and high-resolution mass spectrometry) successfully identified the more polar product as the half-oxidized benzil **2a** and the less polar one as the fully oxidized bisbenzil **3a**. Fluorinated bistolane **1b**, bearing a hexyloxy chain, also undergoes $PdCl_2$-catalyzed C≡C oxidation to give rise to the corresponding benzil **2b** and bisbenzil **3b** in 28% and 21% yield, respectively. When non-fluorinated bistolane **1c** is used as the substrate, the corresponding bisbenzil **3c** is obtained in 40% yield as the major product together with an inseparable mixture.

The mechanism of Pd(II)-catalyzed C≡C oxidation is proposed as follows (Scheme 2) [33]: The catalytic cycle starts with the coordination of the electron-rich C≡C bond to the electron-deficient divalent Pd center, forming the corresponding π-complex (**Int-A**). **Int-A** smoothly undergoes nucleophilic attack by the oxygen atom in DMSO to construct a cationic vinylpalladium(II) species (**Int-B**). Further nucleophilic attack of another DMSO against **Int-B**, followed by elimination of dimethyl sulfide, furnishes a cationic intermediate (**Int-C**). Finally, immediate elimination of dimethyl sulfide and the Pd(II) catalyst gives rise to the corresponding benzil **2**, after which the eliminated Pd(II) catalyst is recycled to provide the oxidation products. The fully oxidized bisbenzil **3** can be yielded by further Pd(II)-catalyzed C≡C oxidation of the half-oxidized benzil **2** via the same catalytic cycle.

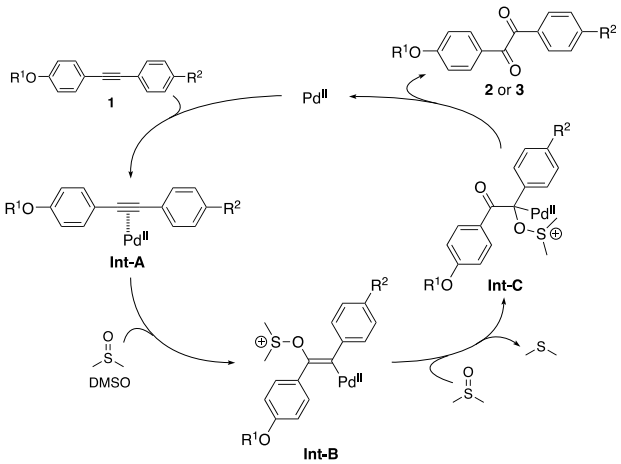

Scheme 2: Proposed mechanism of Pd(II)-catalyzed alkyne oxidation by dimethyl sulfoxide (DMSO).

Considering the proposed reaction mechanism, the successful isolation of the half-oxidized benzil derivatives **2a** and **2b** from the oxidation of fluorinated bistolanes **1a** and **1b**, respectively, may be due to the decreased reactivity of the C≡C bond

toward Pd(II)-catalyzed C≡C oxidation caused by the adjacent electron-deficient fluorinated aromatic ring. To confirm the electron-withdrawing effect of this fluorinated aromatic ring, the electronic charge at the adjacent C≡C bond was calculated by density functional theory (DFT) using the Gaussian 16 (Revision B.01) software package [35]. As typical examples, the molecular geometries of **1a** and **1c** were optimized at the CAM-B3LYP/6-31+G(d) level of theory. The absence of any imaginary frequency in the vibrational analysis proved that the calculated structures are the minima. Figure 3 shows the calculated Mulliken charge distributions of fluorinated **1a** and non-fluorinated **1c**.

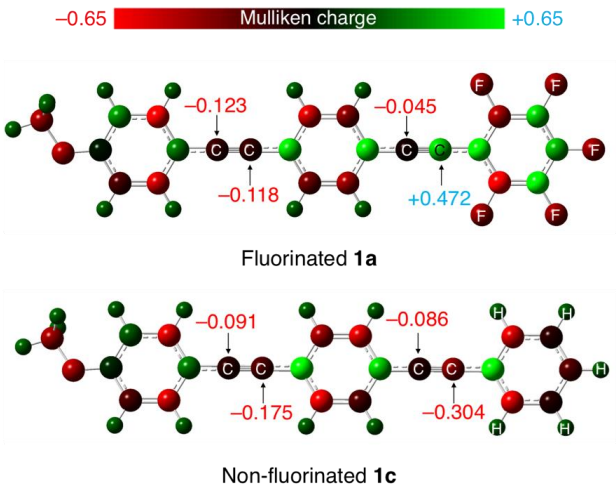

Figure 3: Mulliken charge distributions of fluorinated **1a** and non-fluorinated **1c** obtained from density functional theory calculations [CAM-B3LYP/6-31+G(d) level].

The sp-hybridized carbon adjacent to the fluorinated aromatic ring of **1a** has a largely positive Mulliken charge (+0.472), while that adjacent to the non-fluorinated aromatic ring of **1c** has the opposite negative charge (–0.304). This clearly indicates that the fluorinated aromatic ring retards the Pd(II)-catalyzed oxidation of the adjacent C≡C bond, thereby allowing the isolation of the half-oxidized benzil derivative **2a**. On the basis of this theoretical investigation, the unique reactivities of bistolanes with

fluorinated and non-fluorinated aromatic rings toward oxidation by DMSO can be rationally explained.

Photophysical behavior

Our interest was then directed toward the photophysical properties of benzil and bisbenzil derivatives, which were freshly purified by column chromatography (eluent: hexane/EtOAc = 10/1 for benzil and 5/1 for bisbenzil) and subsequently recrystallized from hexane. The sample solution concentrations in toluene were 1.0×10^{-5} and 1.0×10^{-3} M for the absorption and photoluminescence (PL) measurements, respectively, and the absorption and PL spectra are shown in Figure 4. The photophysical data obtained from these measurements are summarized in Table 1.

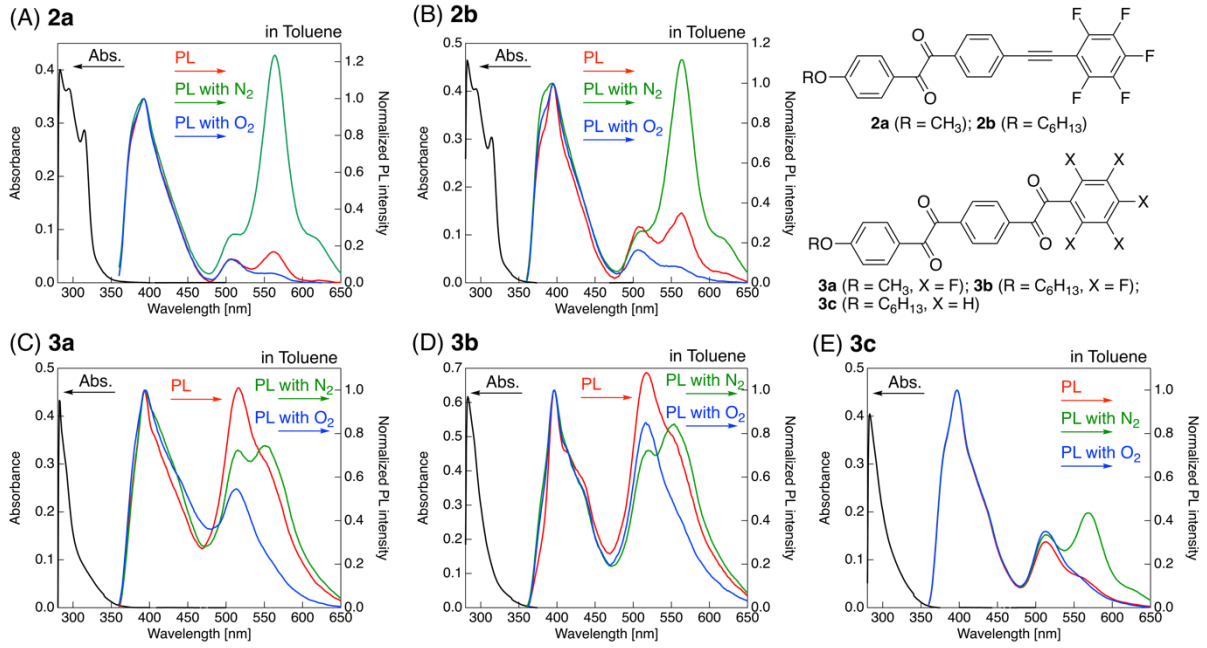

Figure 4: Absorption and PL spectra of (A) **2a**, (B) **2b**, (C) **3a**, (D) **3b**, and (E) **3c** in toluene solution. Concentrations: 1.0×10^{-5} and 1.0×10^{-3} M for absorbance and PL measurements, respectively. Color legend: black: absorption, red: PL as prepared, green: PL under N_2 atmosphere, and blue: PL under O_2 atmosphere.

Table 1: Photophysical data from ultraviolet (UV)-visible absorption and steady-state photoluminescence (PL) measurements[a].

	λ_{abs} [nm] (ε [M^{-1} cm^{-1}])	λ_{PL} [nm][b] (Φ_{PL})[c]	I_{560}/I_{395}		
			pristine	N_2	O_2
2a	295 (28700), 315 (36500), 407 (160)	395, 406sh[d], 507, 563 (0.018)	0.17	1.24	0.05
2b	293 (40500), 314 (30400), 407 (180)	395, 406sh, 507, 563 (0.015)	0.35	1.12	0.08
3a	290 (30500), 405 (180)	393, 406sh, 516, 551 (<0.01)	0.61	0.74	0.19
3b	290 (51200), 405 (212)	396, 412, 517, 554 (<0.01)	0.79	0.84	0.50
3c	290 (29600), 402 (260)	397, 412, 514, 569 (<0.01)	0.14	0.44	0.14

[a]Toluene solution (concentrations: 1.0×10^{-5} and 1.0×10^{-3} M for UV-visible absorption and PL measurements, respectively); [b]Excitation wavelength: 350 nm; [c]Quantum yield measured using a calibrating sphere. Excitation wavelength: 290 nm. [d]Shoulder peak.

The methoxy-substituted fluorinated benzil **2a** in toluene absorbs UV light at 315 and 295 nm with molar extinction coefficients (ε) of 36500 and 28700 M^{-1} cm^{-1}, respectively (Figure 4A). Similarly, the toluene solution of the fluorinated benzil with a hexyloxy chain (**2b**) absorbs UV light at 314 (ε: 30400 M^{-1} cm^{-1}) and 293 nm (ε: 40500 M^{-1} cm^{-1}) (Figure 4B). Both **2a** and **2b** exhibit weak absorption at around 400 nm (ε: ~170 M^{-1} cm^{-1}). As shown in Figures 4C–4E, on the other hand, the bisbenzil derivatives **3a**–**c** show an absorption band at 290 nm (ε: 29600–51200 M^{-1} cm^{-1}) as

the major signal, together with a quite weak absorption band at 402–405 nm (ε: 180–260 M^{-1} cm^{-1}). To gain more information about the slight difference between the absorption behaviors of the benzil and bisbenzil derivatives, DFT and time-dependent DFT (TD-DFT) calculations at the CAM-B3LYP/6-31+G(d) level of theory were performed for fluorinated benzil **2a** and bisbenzil derivative **3a** as representative examples. Figure 5 shows the distributions of molecular orbitals involved in vertical electronic transitions in **2a** and **3a**.

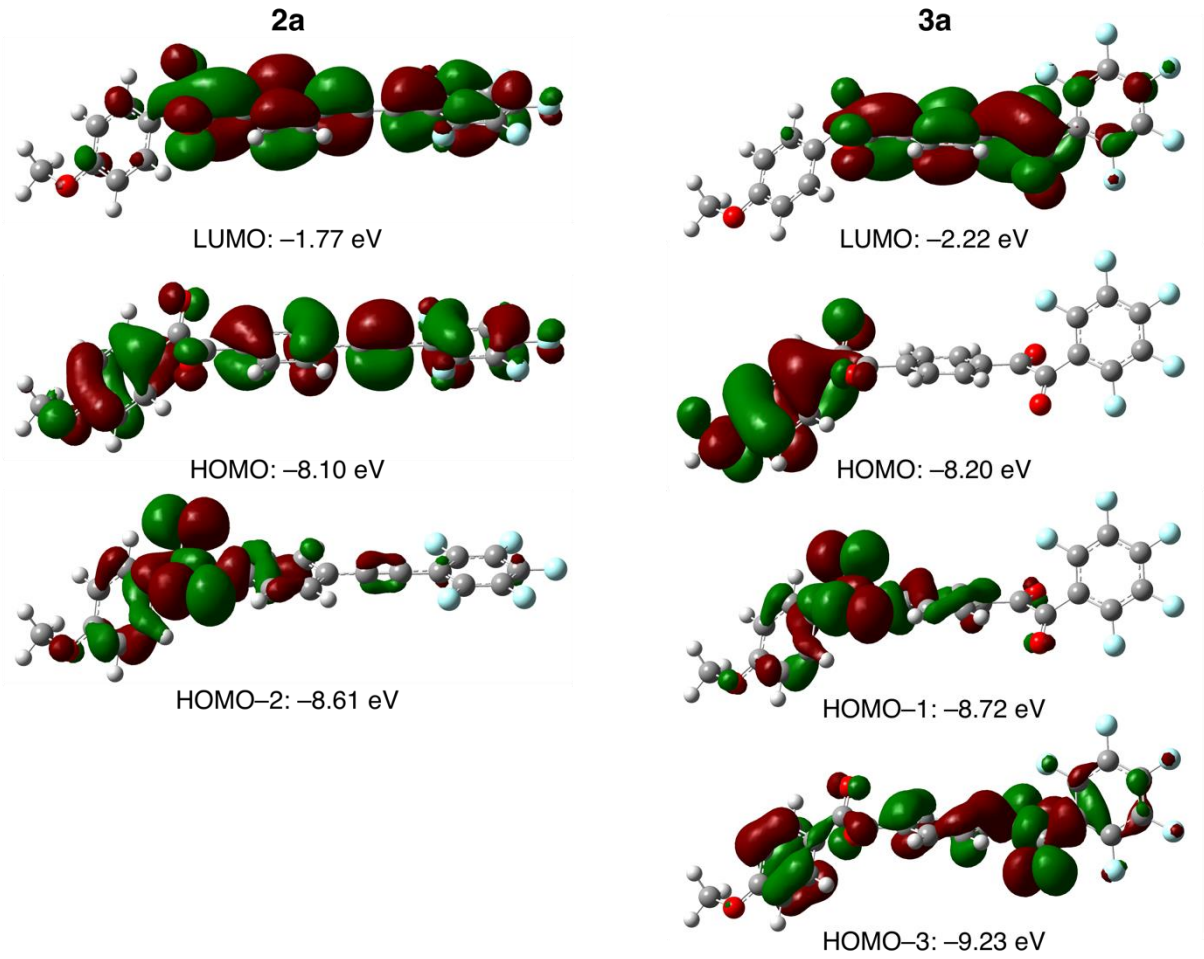

Figure 5: Distributions of molecular orbitals (isosurface value: 0.04 a.u.) involved in vertical electronic transitions in **2a** and **3a** calculated using density functional theory (DFT) and time-dependent DFT at the CAM-B3LYP/6-31+G(d) level (HOMO: highest occupied molecular orbital, LUMO: lowest unoccupied molecular orbital).

The main electronic transition with a relatively large oscillator strength (*f*) in both **2a** and **3a** is the highest occupied molecular orbital (HOMO)→the lowest unoccupied molecular orbital (LUMO) transition. Focusing on the orbital distribution, the HOMO lobe of **2a** covers the entire molecule, while the LUMO lobe is localized at the tolane moiety. In case of **3a**, the HOMO lobe is localized at the methoxy-substituted benzene ring, while the LUMO lobe is localized at the central benzene ring. Accordingly, it can be concluded that the absorption bands at the short-wavelength region (around 290–315 nm) stems from the π-π* transition. The TD-DFT calculation also reveals that n-π* transitions (e.g., HOMO–2→LUMO for **2a** and HOMO–3→LUMO for **3a**) have small values of *f*; thus, the small absorption band at around 400 nm can be safely attributed to a n-π* transition.

Upon irradiation of the toluene solutions of benzil derivatives **2a** and **2b** with a 350-nm UV light, three PL bands at 395, 507, and 563, along with a shoulder signal at around 406 nm, are observed (Figures 4A and 4B). The bisbenzil derivatives, i.e., **3a**–**c**, also show similar PL behavior to the aforementioned benzil analogues: four PL bands with λ_{PL} of 393–397, 406–412, 514–517, and 551–569 nm are observed. To gain more information about the PL process in benzils and bisbenzils, the PL spectra of the toluene solutions (1.0×10^{-3} M) were acquired after bubbling with N_2 or O_2 gas for 30 min. In general, an O_2-saturated environment strongly deactivates the triplet states of specimens; thus, PL emission stems only from fluorescence. On the other hand, elimination of O_2 gas from a solution by bubbling with an inert gas (N_2 or Ar) allows the triplet states to survive for a long lifetime, which leads to an increase in the radiative rate of phosphorescence. Hence, the elimination of O_2 gas from solutions by N_2 gas bubbling (or addition of O_2 gas in solutions) can judge the presence of phosphorescence, as well as the assignment of PL bands. The obtained PL spectra are superimposed on the PL spectra of a pristine sample (Figure 4). Upon bubbling

the solution with N_2 gas for 30 min, a dramatic enhancement of the PL intensities of benzils **2a** and **2b** at λ_{PL} = 563 nm is observed. The PL intensities of bisbenzils **3a–c** at the long-wavelength region between 551 and 569 nm also increase, although the increment rates are not as high as those of **2a** and **2b**. On the contrary, bubbling the toluene solutions of benzil or bisbenzil derivatives with O_2 gas causes the intensity of the long-wavelength PL band to decrease compared with that of the pristine solution, while the other remaining PL bands in the short-wavelength region do not change. Judging from the PL behavior under N_2 or O_2 flow condition, the PL bands at the short-wavelength region around 395 nm and long-wavelength region around 560 nm can be safely considered fluorescence via radiative deactivation from the S_1 excited state to S_0 state and phosphorescence via electronic transition from the T_1 excited state to S_0 state, respectively. Accordingly, fluorinated benzils and bisbenzils show room-temperature phosphorescence in the solution state.

To understand the effects of structural modification (e.g., benzil structure with tolane moiety vs. bisbenzil structure) and incorporation of fluorine atoms on phosphorescence, the ratio between the peak intensities at ~395 and ~560 nm (I_{560}/I_{395}) was quantitatively calculated, and the results are summarized in Table 1. The I_{560}/I_{395} values of benzils **2a** and **2b** under N_2 flow condition increase up to sevenfold compared with those of the corresponding pristine solutions. On the other hand, the increase in the I_{560}/I_{395} values of fluorinated bisbenzil derivatives **3a** and **3b** is low (only 1.1 times) under N_2 flow condition, although the PL intensity of non-fluorinated **3c** increases by approximately three times. Judging from these comprehensive observations, the benzil structure promotes ISC from S_1 to T_1, causing increment phosphorescence, unlike the corresponding bisbenzil scaffold. Moreover, fluorine substituents on the bisbenzil molecules causes significant retardation of ISC, leading to a weak phosphorescence intensity.

Additionally, the quantum yields (Φ_{PL}) of the PL bands in the range of 350–600 nm were acquired using an absolute quantum yield measurement system with a calibrating sphere. All samples have a low Φ_{PL} of less than 0.02 (Table 1), meaning that a vast amount of excited states of all the samples deactivates nonradiatively. At the moment, we cannot determine the cause of the low Φ_{PL} in terms of the molecular properties: for instance, the main pathway of the non-radiative deactivation. To understand the photophysical mechanism of these benzil and bisbenzil derivatives, further experimental study of the excited-state dynamics is necessary and ongoing by us.

Conclusion

In this article, we described the design and synthesis of benzil- or bisbenzil-based room-temperature phosphorescent molecules via a simple oxidation protocol for fluorescent bistolane derivatives. Non-fluorinated bistolane derivatives exclusively yielded the corresponding products with a bisbenzil scaffold, whereas the use of fluorinated bistolane derivatives as the starting materials provided not only mono-oxidized benzil derivatives bearing a fluorinated tolane scaffold, but also bis-oxidized bisbenzil derivatives. Based on theoretical calculations, the selective formation of the fluorinated analogues stemmed from the slight modulation of the charge distribution at the alkyne moiety of the reactant induced by electron-withdrawing fluorine atoms. Evaluation of the photophysical behaviors of benzils and bisbenzils through several PL measurements under N_2 and O_2 flow conditions probed the successful room-temperature phosphorescence of the compounds in toluene solution. The achievement of our ongoing study of the excited state dynamics of the benzil and

bisbenzil derivatives would provide promising knowledge to develop environmentally benign pure organic phosphorescent materials.

Supporting Information

Experimental procedures for the synthesis and characterization of fluorinated benzils **2a** and **2b**, fluorinated bisbenzils **3a** and **3b**, and non-fluorinated bisbenzil **3c**. ^{1}H, ^{13}C, and ^{19}F NMR spectra of **2a**, **2b**, and **3a**–**c**. Cartesian coordinates of the optimized geometries of **1a**, **1c**, **2a**, and **3a** obtained from DFT calculations.

Supporting Information File 1:

File Name: SI_YAMADA.pdf

File Format: PDF

Title: Supporting Information

Funding

The following sources of funding are acknowledged: Japan Society for the Promotion of Science (JSPS) KAKENHI Grant-in-Aid for Scientific Research (C) (Grant No. JP18K05262) and the AIST Nanocharacterization Facility (ANCF) platform as a part of a program of the “Nanotechnology Platform” of the Ministry of Education, Culture, Sports, Science and Technology (MEXT), Japan.

References

1. Singh, H.; Tiwari, K.; Tiwari, R.; Pramanik, S. K.; Das, A. *Chem. Rev.,* **2019,** *119,* 11718–11760.

2. Mei, J.; Huang, Y.; Tian, H. *ACS Appl. Mater. Interfaces*, **2018,** *10*, 12217–12261.

3. Chen, X.; Wang, F.; Hyun, J. Y.; Wie, T.; Qiang, J.; Ren, X.; Shin, I.; Yoon, J. *Chem. Soc. Rev.*, **2016**, *45*, 2976–3016.

4. Ma, Y.; Zhang, Y.; Yu, W. M. *J. Mater. Chem. C*, **2019**, *7*, 13662–13679.

5. Yersin, H., Ed. *Highly Efficient OLEDs: Materials Based on Thermally Activated Delayed Fluorescence*; Wiley-VCH: Weinheim, Germany, 2019.

6. Gaspar, D. J.; Polikarpov, E., Eds. *OLED Fundamentals: Materials, Devices, and Processing of Organic Light-Emitting Diodes*; CRC Press: Boca Raton, 2015.

7. Su, L.; Fan, X.; Yin, T.; Wang, H.; Li, Y.; Liu, F.; Li, J.; Zhang, H.; Xie, H., *Adv. Opt. Mater.*, **2020**, *8*, 1900978 (DOI: 10.1002/adom.201900978).

8. Ostroverkhova, O., *Chem. Rev.*, **2016**, *116*, 13279–13412.

9. Ronda, C. R. Emission and Excitation Mechanisms of Phosphors. In *Luminescence: From Theory to Applications*; Ronda, C., Ed.; Wiley-VCH: Weinheim, Germany, 2007; pp 1–30.

10. Yersin, H.; Rausch, A. F.; Czerwieniec, R. Organometallic Emitters for OLEDs: Triplet Harvesting, Singlet Harvesting, Case Structures, and Trends. In *Physics of Organic Semiconductors*; Brütting, W.; Adachi, C., Eds.; Wiley-VCH: Weinheim, Germany, 2012; pp 371–424.

11. Wang, W.; Zhang, Y.; Jin, W. J. *Coord. Chem. Rev.*, **2020**, *404*, 213107 (DOI: 10.1016/j.ccr.2019.213107).

12. Zhang, G.; Liu, Z.; Bian, Z.; Huang, C. *Front. Chem.* (Lausanne, Switz.), **2019**, *7*, 305 (DOI: 10.3389/fchem.2019.00305).

13. Qu, G.; Zhang, Y.; Ma, X. *Chin. Chem. Lett.*, **2019**, *30*, 1809–1814.

14. Crosby, G. A. *Acc. Chem. Res.*, **1975**, *8*, 231–238.

15. Baldo, M. A.; Lamansky, S.; Burrows, P. E.; Thompson, M. E.; Forrest, S. R. *Appl. Phys. Chem.*, **1999**, *75*, 4–6.

16. Adachi, C.; Baldo, M. A.; Forrest, S. R.; Thompson, M. E. *Appl. Phys. Lett.*, **2000**, *77*, 904–906.

17. Baldo, M. A.; O'Brien, D. F.; You, Y.; Shoustikov, A.; Sibley, S.; Thompson, M. E.; Forrest, S. R. *Nature*, **1998**, *395*, 151–154.

18. Yam, V. W.-W.; Wong, K. M.-C.; Hung, L.-L.; Zhu, N. *Angew. Chem., Int. Ed.*, **2005**, *44*, 3107–3110.

19. Yamada, S.; Yamaguchi, S.; Tsutsumi, O. *J. Mater. Chem. C*, **2017**, *5*, 7977–7984.

20. Fujisawa, K.; Kawakami, N.; Onishi, Y.; Izumi, Y.; Tamai, S.; Sugimoto, N.; Tsutsumi, O. *J. Mater. Chem. C*, **2013**, *1*, 5359–5366.

21. Seki, T.; Takamatsu, Y.; Ito, H. *J. Am. Chem. Soc.*, **2016**, *138*, 6252–6260.

22. Kenry; Chen, C.; Liu, B. *Nat. Commun.*, **2019**, *10*, 2111 (DOI: 10.1038/s41467-019-10033-2).

23. Yuan, W. Z.; Shen, X. Y.; Zhao, H.; Lam, J. W. Y.; Tang, L.; Lu, P.; Wang, C.; Liu, Y.; Wang, X.; Zheng, Q.; Sun, J. Z.; Ma, Y.; Tang, B. Z. *J. Phys. Chem. C*, **2010**, *114*, 6090–6099.

24. Bolton, O.; Lee, K.; Kim, H.-J.; Lin, K. Y.; Kim, J. *Nat. Chem.*, **2011**, *3*, 205–211.

25. Zhao, W.; He, Z.; Lam, J. W. Y.; Peng, Q.; Ma, H.; Shuai, Z.; Bai, G.; Hao, J.; Tang, B. Z. *Chem*, **2016**, *1*, 592–692.

26. Lower, S. K.; El-Sayed, M. A. *Chem. Rev.*, **1966**, *66*, 199–241.

27. Morita, M.; Yamada, S.; Agou, T.; Kubota, T.; Konno, T. *Appl. Sci.*, **2019**, *9*, 1905 (DOI: 103390/1pp9091905).

28. Yamada, S.; Miyano, K.; Agou, T.; Kubota, T.; Konno, T. *Crystals*, **2019**, *9*, 195 (DOI: 103390/cryst9040195).

29. Yamada, S.; Tanaka, T.; Ichikawa, T.; Konno, T. *ACS Omega*, **2019**, *4*, 3922–3932.

30. Yamada, S.; Morita, M.; Agou, T.; Kubota, T.; Ichikawa, T.; Konno, T. *Org. Biomol. Chem.*, **2018**, *16*, 5609–5617.

31. Yamada, S.; Miyano, K.; Konno, T.; Agou, T.; Kubota, T.; Hosokai, T. *Org. Biomol. Chem.*, **2017**, *15*, 5949–5958.

32. Gong, Y. Y.; Tan, Y. Q.; Li, H.; Zhang, Y. R.; Yuan, W. Z.; Zhang, Y. M.; Sun, J. Z.; Tang, B. Z. *Sci. China: Chem.*, **2013**, *56*, 1183–1186.

33. Muzart, J. *J. Mol. Catal. A: Chem.*, **2011**, *338*, 7–17.

34. Chi, K.-W.; Yusubov, M. S.; Filimonov, V. D. *Synth. Commun.*, **1994**, *24*, 2119–2122.

35. Frisch, M. J.; Trucks, G. W.; Schlegel, H. B.; Scuseria, G. E.; Robb, M. A.; Cheeseman, J. R., Scalmani, G.; Barone, V.; Petersson, G. A.; Nakatsuji, H.; Li, X.; Caricato, M.; Marenich, A. V.; Bloino, J.; Janesko, B. G.; Gomperts, R.; Mennucci, B.; Hratchian, H. P.; Ortiz, J. V.; Izmaylov, A. F.; Sonnenberg, J. L.; Williams-Young, D.; Ding, F.; Lipparini, F.; Egidi, F.; Goings, J.; Peng, B.; Petrone, A.; Henderson, T.; Ranasinghe, D.; Zakrzewski, V. G.; Gao, J.; Rega, N.; Zheng, G.; Liang, W.; Hada, M.; Ehara, M.; Toyota, K.; Fukuda, R.; Hasegawa, J.; Ishida, M.; Nakajima, T.; Honda, Y.; Kitao, O.; Nakai, H.; Vreven, T.; Throssell, K.; Montgomery, J. A., Jr.; Peralta, J. E.; Ogliaro, F.; Bearpark, M. J.; Heyd, J. J.; Brothers, E. N.; Kudin, K. N.; Staroverov, V. N.; Keith, T. A.; Kobayashi, R.; Normand, J.; Raghavachari, K.; Rendell, A. P.; Burant, J. C.; Iyengar, S. S.; Tomasi, J.; Cossi, M.; Millam, J. M.; Klene, M.; Adamo, C.; Cammi, R.; Ochterski, J. W.; Martin, R. L.; Morokuma, K.; Farkas, O.; Foresman, J. B.; Fox, D. J. *Gaussian 16,* Revision B.01; Gaussian, Inc., Wallingford, CT, USA, 2016.